Direct numerical simulations of shock-scalar mixing interaction

Radouan Boukharfane, Zakaria Bouali, Arnaud Mura
Institut PPRIME - UPR 3346 - CNRS - ISAE-ENSMA - Université de Poitiers
BP 40109, 86961 Futuroscope, France

1 Introduction

Due to the short residence time of air in supersonic combustors, achieving efficient mixing in compressible turbulent reactive flows is crucial for the design of supersonic ramjet (Scramjet) engines. In this respect, improving the understanding of shock-scalar mixing interactions is of fundamental importance for such supersonic combustion applications. In these compressible flows, the interaction between turbulence and shock wave is reciprocal, and the coupling between them very strong. Amplification of velocity fluctuations and substantial changes in turbulence characteristic length scales are the most important outcomes of this interaction, which may deeply influence scalar mixing between fuel and oxidizer [1]. A basic understanding of the physics of such complex interactions has already been obtained through the analysis of relevant simplified flow configurations, including (i) shock wave propagating through density-stratified media [2], (ii) shock wave-mixing layer interaction [3], and (iii) shock wave-vortex interaction [4]. The primary goal of the present study is to extend previous analyses to the case of shock-scalar mixing interaction, which is directly relevant to supersonic combustion applications. The turbulent mixing of a passive (i.e., inert) scalar in the presence of a shock wave are thus investigated with a special focus on the transport equations of the variance and mean scalar dissipation rate (SDR) of the mixture fraction.

2 Numerical setup

A schematic view of the computed flow is depicted in Fig. 1. The numerical simulations are performed with a flow solver (CREAMS) that has been previously described and thoroughly verified on several computational benchmarks [5]. For the purpose of the present study, the standard set of conservation equations is supplemented with an additional scalar transport equation:

$$\frac{\partial}{\partial t}(\rho\xi) + \frac{\partial}{\partial x_i}\left(\rho u_i \xi - \rho D \frac{\partial \xi}{\partial x_i}\right) = 0 \tag{1}$$

The quantity ξ denotes a non-reactive scalar bounded between zero and unity, the diffusivity of which is set equal to the thermal diffusivity, i.e., $D = a_T$ (unity Lewis number approximation). The CREAMS solver combines the use of a seventh-order accurate Weighted Essentially Non-Oscillatory (WENO7) scheme with high-precision finite difference schemes. Temporal integration is performed with a third-order Runge-Kutta algorithm. The reader may refer to recent references [6, 7] for further details.

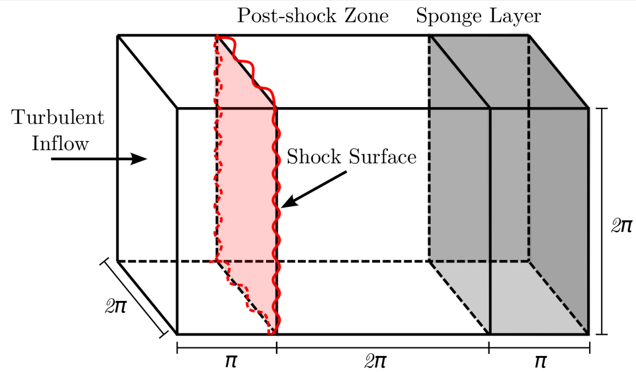

Figure 1: Schematic of the numerical setup.

The computational mesh is uniform in transverse directions whereas computational nodes are clustered in the vicinity of the shock along the streamwise direction. A sponge layer is used to damp out the possible reflection of pressure fluctuations at the outlet [8]. The numerical simulation of such spatially-evolving turbulent flows rises severe challenges, e.g., it is required to prescribe time-dependent turbulent inflow conditions at the upstream boundary and the corresponding inflow must be as realistic as possible. In the present study, the inflow turbulence is generated using the procedure proposed by Ristorcelli and Blaisdell [9]: the velocity spectra is thus settled from $E(k) \sim k^4 exp(-2k^2/k_0^2)$, with k_0 the wavenumber at the peak energy, and allowed to decay temporally until the desired values of the turbulent Mach number M_t and Taylor microscale Reynolds number Re_λ are reached. Then, an instantaneous realization of the flow field is selected as the inflow of the shock-turbulence interaction problem and we make use of the Taylor's hypothesis to specify the time-dependent inflow turbulence. This simulation of isotropic turbulence is performed on a uniform multi-periodic computational grid, which has the dimension of $n\pi \times 2\pi \times 2\pi$. The value of the parameter n is chosen to obtain an inflow data sequence that is sufficiently large to feed the computational domain of Fig. 1 with unduplicated isotropic turbulence for several flow-through (residence) times ($n = 16$ in this work). The scalar fields $\xi(\boldsymbol{x}, t = 0)$ are initialized using the spectral procedure described by Reveillon [10] with a prescribed level of fluctuations (i.e., variance $\widetilde{\xi''^2}$) and a characteristic size l_ξ that is set equal to the turbulence integral length scale l_T. This method allows to generate isotropic fluctuating scalar fields for various values of the segregation-rate and length scale l_ξ. For the considered value of the turbulence Reynolds number, $450 \times 128 \times 128$ grid points are required, and for any variable ψ the mean value is obtained by averaging the data along homogeneous directions (i.e., $y - z$ planes) and over time $\Delta t = 80/(k_0 u_{1,\mathrm{u}})$ with $u_{1,\mathrm{u}}$ the mean flow inlet velocity. Numerical simulations are performed for various values of the mean inlet Mach number M ranging from 1.7 to 2.7.

2 Reynolds stresses and vorticity variance evolutions

Figure 2 displays the evolution of Reynolds stresses and vorticity variances. As predicted by the Linear Interaction Approximation (LIA), the increase of the Mach number M leads to the amplification of both the streamwise and transverse Reynolds stress components. All the components of velocity fluctuations are augmented during the shock interaction; the transverse vorticity is directly amplified at the shock location and then decays monotonically due to viscous dissipation. The velocity fluctuations are axisymmetric behind the shock wave and the return-to-isotropy effects remain negligible over the decay period. The streamwise vorticity is initially unaffected by the shock, but then quickly increases until it equilibrates with the transverse components. The general trends issued from the present set of DNS data thus appear to be fully consistent with other data available from the literature [8, 11, 12].

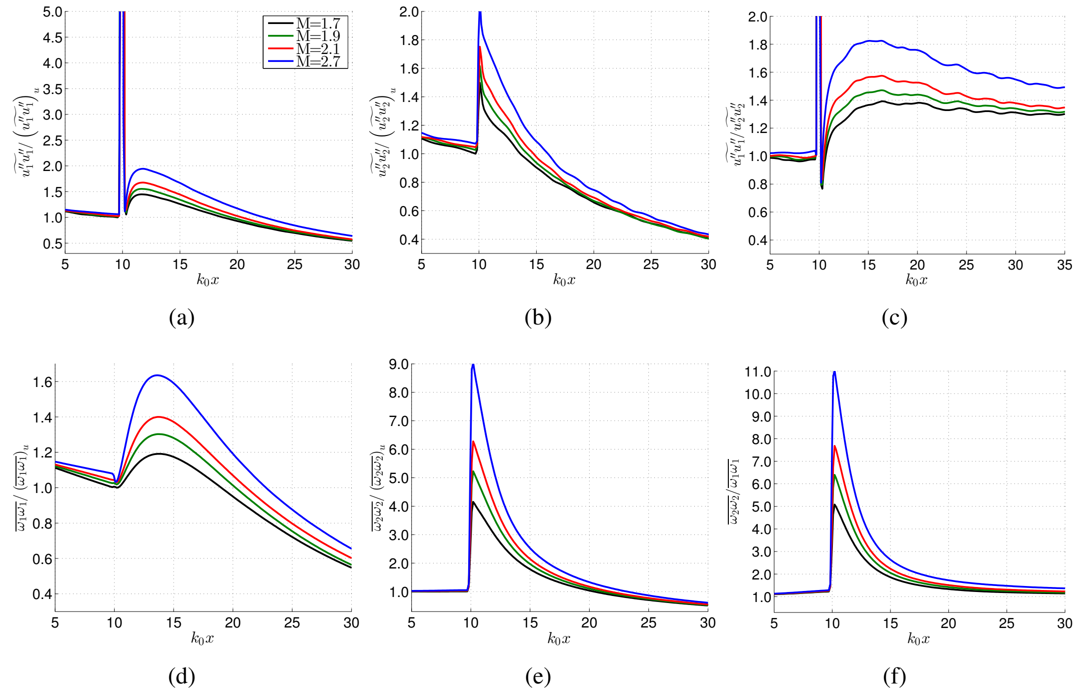

Figure 2: (a) and (b): evolutions of normalised Reynolds stress components, (d) and (e): evolutions of normalised vorticity variances, (c) and (f): evolutions of anisotropy levels.

3 Evolution of the scalar variance and mean scalar dissipation rate

The scalar mixing is now analyzed in the light of the scalar variance evolution. In a variable density flow the transport equation of the scalar variance $\widetilde{\xi''^2}$ may be written as follows

$$\frac{\partial}{\partial t}\left(\overline{\rho}\widetilde{\xi''^2}\right) = -\underbrace{\frac{\partial}{\partial x_k}\left(\overline{\rho}\widetilde{u}_k\widetilde{\xi''^2}\right)}_{\text{(TII)}} + \underbrace{\frac{\partial}{\partial x_k}\left(\overline{\rho D\frac{\partial \xi''^2}{\partial x_k}}\right)}_{\text{(TIII)}} - \underbrace{\frac{\partial}{\partial x_k}\left(\overline{\rho u_k''\xi''^2}\right)}_{\text{(TIV)}}$$
$$-\underbrace{2\overline{\rho D\frac{\partial \xi''}{\partial x_k}\frac{\partial \xi''}{\partial x_k}}}_{\text{(TV)}} - \underbrace{2\overline{\rho u_k''\xi''}\frac{\partial \widetilde{\xi}}{\partial x_k}}_{\text{(TVI)}} + \underbrace{2\overline{\xi''\frac{\partial}{\partial x_k}\left(\rho D\frac{\partial \widetilde{\xi}}{\partial x_k}\right)}}_{\text{(TVII)}} \tag{2}$$

In Eq. (2) the term (TII) corresponds to mean advection. In the statistically homogeneous case, i.e., without shock, it reduces to a surface term, and its integral over the whole computational domain is zero: it does not modify the scalar variance level. The same conclusion holds for (TIII) and (TIV). Since there is no gradient of mean concentration in such homogeneous cases, (TVI) and (TVII) will also cancel, and only the scalar

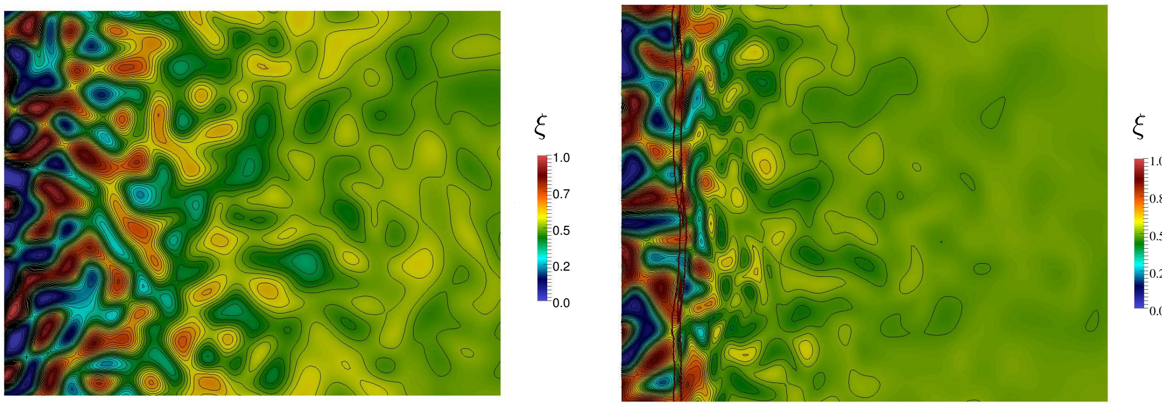

Figure 3: Instantaneous snapshots of the scalar field (slice at $z = \pi$), left: without shock, right: with shock.

dissipation rate (SDR) term (TV) will be non-zero in the right-hand side of Eq. (2). In the presence of a shock, the flow is no longer homogeneous along the streamwise direction and all terms must be considered.

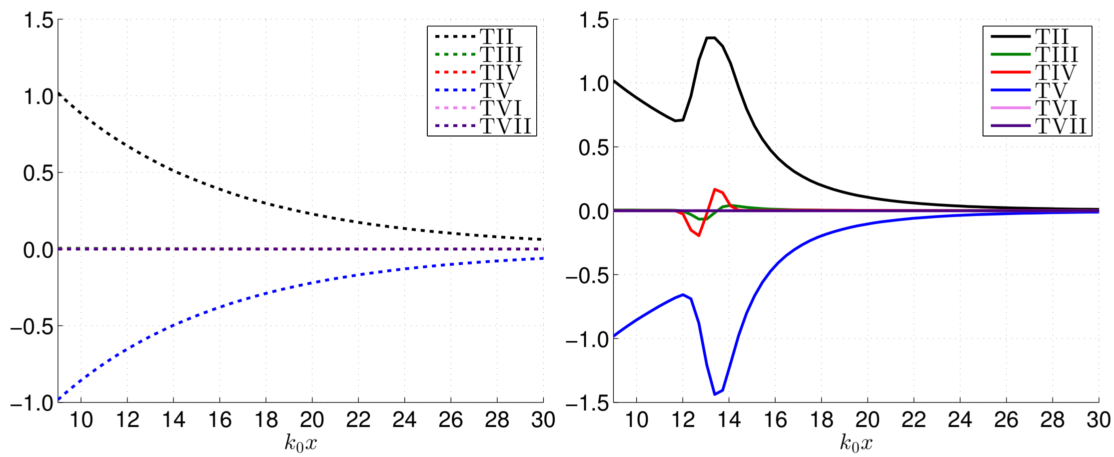

Figure 4: Budgets of scalar variance for $M = 2.0$. Dashed lines correspond to the unshocked case.

Figure 3 illustrates the effect of the shock wave on the scalar fluctuations decay. As expected, the scalar variance decreases in both cases, but the decay is intensified through the interaction with the shock. This is made clearer in Fig. 4 that reports different terms of Eq.(2) normalised by $\rho_u u_{1,u}(\widetilde{\xi''^2})_u/l_T$. As seen from Fig. 4, the turbulent SDR, i.e., (TV), is negative-definite and monotonically reduces the scalar variance, corresponding to the scalar field homogenisation through molecular diffusion effects. This term increases after the shock, thus enhancing scalar mixing processes, see Fig. 4. The right side of Fig. 5 displays the spatial evolution of (SDR) for shocked and unshocked cases, it is seen that the shocked region undergoes a rapid reduction in the magnitude of spatially averaged scalar dissipation rate thus confirming the enhancement of mixing processes in comparison with the unshocked case.

We consider now the mean SDR transport equation and special attention is paid on the turbulence-scalar interaction (TSI) term, that corresponds to the sum of terms (V), (VI) and (VII) in reference [14]. It writes: (TSI) $= -2\overline{\rho N_\xi^{ij}\partial u_j/\partial x_i} = -2\overline{\rho N_\xi \sum_{k=1}^{k=3} \lambda_k \cos^2(\theta_k)}$, with $N_\xi^{ij} = D \cdot \partial\xi/\partial x_i \cdot \partial\xi/\partial x_j$ the SDR tensor.

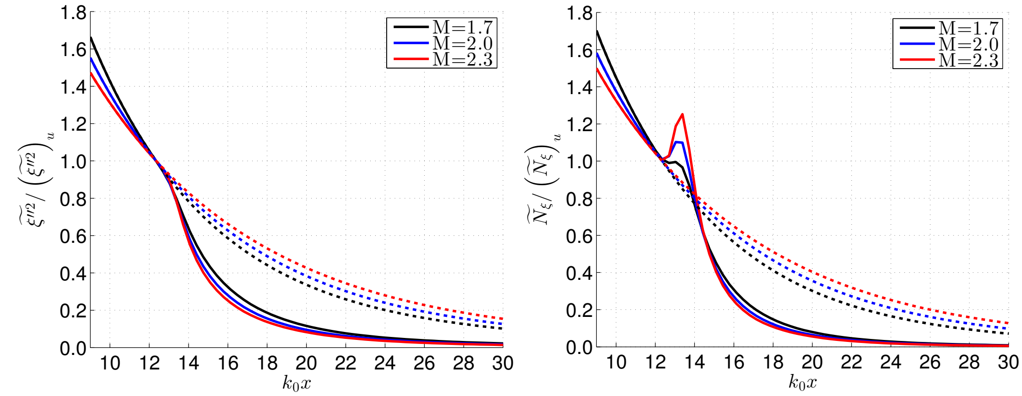

Figure 5: Evolutions of scalar variance and mean SDR. Dashed lines correspond to the unshocked case.

The quantities λ_i denote the eigenvalues of the strain-rate tensor S_{ij}. Since S_{ij} is a symmetric second rank tensor, they are real numbers, ordered by $\lambda_1 > \lambda_2 > \lambda_3$, where $\lambda_1 > 0$ represents the most extensive principal direction and $\lambda_3 < 0$ corresponds to the most compressive principal direction. The (TSI) term reflects the production (or dissipation) of scalar gradients by the action of turbulence. Alignment statistics between strain and scalar gradient are reported in Fig. 6. Scalar gradient is found to be mostly aligned with the strain-rate principal direction of compression. A remarkable point is that the probability to be perpendicular with the intermediate direction is significantly increased in the vicinity of the shock-wave. Other results, which are not reported herein just for the sake of conciseness, confirm the strong influence of the shock wave on turbulent mixing. Especially, the statistics of λ_2, which reflects the intensity of turbulent transfer, are significantly modified by the shock wave.

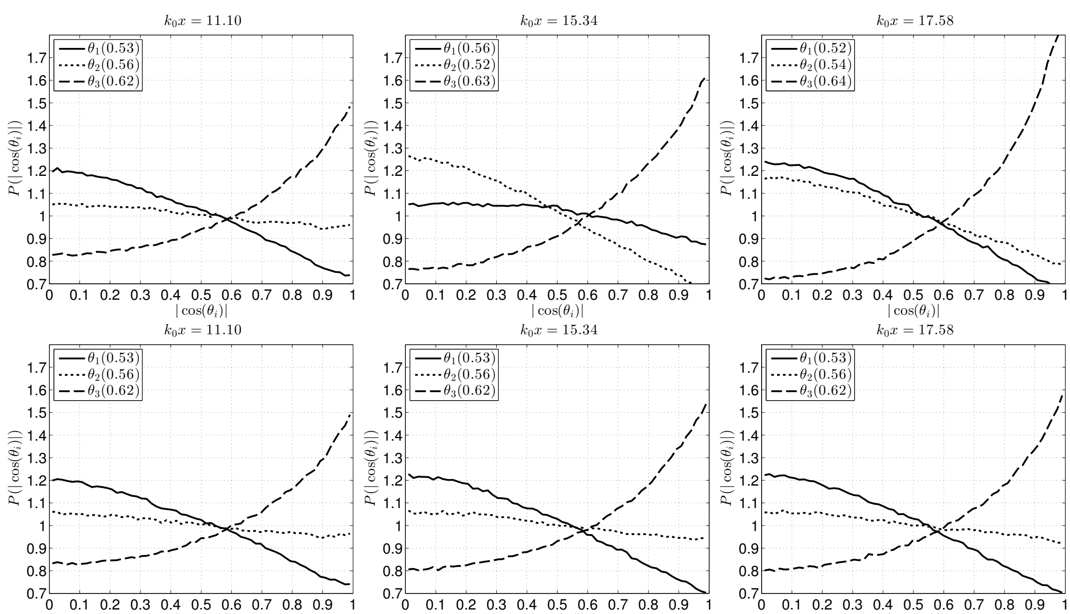

Figure 6: PDFs of the orientation between the scalar gradient and the strain-rate eigenvectors at three locations. Images on the top correspond to the shocked case, on the bottom to the unshocked case.

4 Conclusion

Direct numerical simulations are conducted to analyse the effect of a stationary normal shock on the scalar mixing processes. The spatial evolution of the scalar variance and its dissipation rate are studied and compared for both the shocked and unshocked cases for various Mach number values. The interaction with the shock is found to (i) generate strong vortical motion originating along the shock, and (ii) intensify significantly the mixing processes. The PDFs that characterize the alignement of the scalar gradient with the principal directions of the strain-rate tensor are significantly modified just downstream of the shock, with a significant decrease of the characteristic length of scalar pockets l_ξ and associated mixing enhancement.

Acknowledgements: This work is part of the PhD thesis of R. Boukharfane, financially supported by Region Poitou-Charentes. It was granted access to the resources of IDRIS under the allocations x20142a0912 and x20142b7251 made by GENCI.

References

[1] Huh H., Driscoll J.F. (1996), Shock-wave-enhancement of the mixing and the stability limits of supersonic hydrogen-air jet flames, Proc. Combust. Inst., vol. 26, pp. 2933-2939.

[2] Layes G., Le Métayer O. (2007), Quantitative numerical and experimental studies of the shock accelerated heterogeneous bubbles motion, Phys. Fluids, vol. 19, pp. 042105.

[3] Morgan B., Duraisamy K., Nguyen N., Kawai S., Lele, S.K. (2013), Flow physics and RANS modelling of oblique shock/turbulent boundary layer interaction, J. Fluid Mech., vol. 729, pp. 231-284.

[4] Grasso F., Pirozzoli S. (2000), Shock-wave–vortex interactions: shock and vortex deformations, and sound production, Theor. Comput. Fluid Dyn., vol. 13, pp. 421-456.

[5] Martinez Ferrer P.J., Buttay R., Lehnasch G., Mura A. (2014), A detailed verification procedure for compressible reactive multicomponent Navier-Stokes solvers, Comput. Fluids, vol. 89, pp. 88-210.

[6] Buttay R., Lehnasch G., Mura A. (2016), Analysis of small-scale scalar mixing processes in highly under-expanded jets, Shock Waves, vol. 26, pp.193-212.

[7] Martinez Ferrer P.J., Lehnasch G., Mura A. (2017), Compressibility and heat release effects in high-speed reactive mixing layers, Combust. Flame, vol. 177 (in press).

[8] Larsson J., Lele S.K. (2009), Direct numerical simulation of canonical shock/turbulence interaction, Phys. Fluids, vol. 21, pp. 126101.

[9] Ristorcelli J.R., Blaisdell G.A. (1997), Consistent initial conditions for the DNS of compressible turbulence, Phys. Fluids, vol. 9, pp. 4-6.

[10] Reveillon J. (2005), Numerical procedures to generate and to visualize flow fields from analytical or experimental statistics, J. Flow Vis. Image Proc., vol. 12, pp. 251-269.

[11] Mahesh K., Lee S., Lele S.K., Moin P. (1995), The interaction of an isotropic field of acoustic waves with a shock wave, J. Fluid Mech., vol. 300, pp. 383-407.

[12] Livescu D., Ryu J. (2016), Vorticity dynamics after the shock–turbulence interaction, Shock Waves, vol. 26, pp. 241-251.

[13] Mura A., Borghi R. (2003), Towards an extended scalar dissipation equation for turbulent premixed combustion, Combust. Flame, vol. 133, pp. 193-196.

[14] Gomet L., Robin V., Mura A. (2012), Influence of residence and scalar mixing time scales in non-premixed combustion in supersonic turbulent flows, Combust. Sci. Technol., vol. 184, pp. 1471-1501.